The impact of artificial selection on morphological integration in the appendicular skeleton of domestic horses

Pauline Hanot,[1] (iD) Anthony Herrel,[2] (iD) Claude Guintard[3] and Raphaël Cornette[4]

[1]UMR 7209 Archéozoologie et Archéobotanique: Sociétés, Pratiques et Environnements (CNRS, MNHN), Muséum national d'Histoire naturelle, Sorbonne Universités, Paris, France
[2]UMR 7179 Mécanismes Adaptatifs et Évolution (CNRS, MNHN), Muséum national d'Histoire naturelle, Sorbonne Universités, Paris, France
[3]École Nationale Vétérinaire, de l'Agroalimentaire et de l'Alimentation, Nantes Atlantique – ONIRIS, Nantes Cedex 03, France
[4]UMR 7205 Institut de Systématique, Évolution, Biodiversité (CNRS, MNHN, UPMC, EPHE), Muséum national d'Histoire naturelle, Sorbonne Universités, Paris, France

Abstract

The relationships between the different component parts of organisms, such as the sharing of common development or function, produce a coordinated variation between the different traits. This morphological integration contributes to drive or constrain morphological variation and thus impacts phenotypic diversification. Artificial selection is known to contribute significantly to phenotypic diversification of domestic species. However, little attention has been paid to its potential impact on integration patterns. This study explores the patterns of integration in the limb bones of different horse breeds, using 3D geometric morphometrics. The domestic horse is known to have been strongly impacted by artificial selection, and was often selected for functional traits. Our results confirm that morphological integration among bones within the same limb is strong and apparently partly produced by functional factors. Most importantly, they reveal that artificial selection, which led to the diversification of domestic horses, impacts covariation patterns. The influence of selection on the patterns of covariation varies along the limbs and modulates bone shape, likely due to a differential ligament or muscle development. These results highlight that, in addition to not being constrained by a strong morphological integration, artificial selection has modulated the covariation patterns according to the locomotor specificities of the breeds. More broadly, it illustrates the interest in studying how micro-evolutionary processes impact covariation patterns and consequently contribute to morphological diversification of domestic species.

Key words: appendicular skeleton; artificial selection; functional morphology; horse breeds; morphological integration; three-dimensional geometric morphometrics.

Introduction

It has been generally accepted that morphological changes are influenced by interactions between the different component parts of organisms (Wagner & Altenberg, 1996; Hallgrímsson et al. 2002). These relationships are produced by biological processes such as the sharing of common development or function (Olson & Miller, 1951, 1958; Magwene, 2001; Marroig & Cheverud, 2001; Wagner et al. 2007; Hallgrímsson et al. 2009; Klingenberg, 2009; Goswami et al. 2014). The tendency of morphological traits to vary in a coordinated manner (or covariation) is defined as morphological integration (Olson & Miller, 1951, 1958; Van Valen, 1965). This biological organization of organisms can be conserved and translated into patterns of evolutionary integration (Cheverud, 1982). Thus, morphological integration contributes to drive or constrain phenotypic diversification.

The correlation of morphometric variables is usually used to explore morphological integration (Mitteroecker & Bookstein, 2007; Goswami & Polly, 2010; Klingenberg, 2013; Klingenberg, 2014; Adams, 2016). Covariation patterns among tetrapod limb bones have been frequently explored,

notably in order to identify functional units (Hallgrímsson et al. 2002; Young & Hallgrímsson, 2005; Lawler, 2008; Rolian, 2009; Young et al. 2010; Goswami et al. 2014; Martín-Serra et al. 2015). It is generally considered that morphological integration between bones within a single limb is the result of functional interactions (Hallgrímsson et al. 2002; Young & Hallgrímsson, 2005; Fabre et al. 2014; Martín-Serra et al. 2015) because they are involved in common functional tasks through shared articular surfaces, muscles or ligaments. Thus, the study of covariation among bones of a same limb can highlight their functional interactions and thus inform us about the locomotor specificities of animals.

Here we focus on a species which displays wide morphological variability: the domestic horse. To suit human activities, domestic horses (*Equus caballus*) have been moulded through selection for conformation, gaits or performance (e.g. for sprinting speed or jumping ability). This selective breeding is known to have largely impacted their morphological and functional traits with the aim of developing specific phenotypes (Musset, 1917; Mulliez, 1983; Lizet, 1989; Denis, 2012). This diversity mainly results from the standardization of a large range of various breeds, started in the 18th century (Mulliez, 1983; Denis, 2012). Indeed, the ancient morphological types of horses were forged by a long-term regional differentiation of local populations, often adapted to their environment. Subsequently, some of the characteristics resulting from the regional and natural variation were used to establish a cross-breeding program (Denis, 2012). Morphological standards were defined and a strong artificial selection was performed to produce the current breeds. Hence, it is considered that the genetic isolation of the standardized breeds is due more to deliberate anthropic choices than to geographic isolation (Sponenberg & Christman, 1995; Sponenberg, 2000). Thus, artificial breeding appears as the main source of morphological diversification in domestic horses.

Despite the fact that the role of artificial selection on the phenotype of domestic species is well known (Darwin, 1868), little attention has been paid to morphological integration patterns in these domestic organisms (Drake & Klingenberg, 2010). Moreover, whereas the interspecific differences in covariation patterns are generally examined, almost no data exist on the comparison of domestic breeds. In this study we explore the patterns of integration in the appendicular skeleton of various horse breeds. Due to the fact that artificial breeding of horses is largely based on functional aspects, morphological traits that underlie these functions, and thus probably integration patterns, are expected to have evolved with selection. Indeed, the patterns of integration are supposed partly to reflect functional associations among traits (Cheverud, 1982; Wagner & Altenberg, 1996). Consequently, we hypothesize that functional variations among breeds are reflected in differences

in covariation patterns among musculoskeletal traits. On the other hand, the appendicular skeleton of horses has previously been demonstrated to be a strongly integrated system (Hanot et al. 2017b). This raises the issue of the potential impact on evolvability of a strong morphological integration which could be considered as restricting shape changes (Goswami & Polly, 2010). To explore these questions, we investigate differences in covariation patterns between different breeds and the principal areas of covariation of each bone are described to understand the underlying causes of covariation. This study also allows us to explore whether the impact of the selective breeding differs according to the different pairs of bones in order to understand better the factors governing integration in the appendicular skeleton of horses.

Materials and methods

Materials

The dataset includes the complete or partial skeletons of 35 domestic horses (*Equus caballus*) housed in the collections of several European institutions (Table 1) and selected to be representative of a large morphological diversity in terms of breeds and functions (i.e. racehorses, draft horses, Shetland ponies, Icelandic ponies, Camargue, Pottok, Mongol horses). The sample consists of both males and females. Only adult specimens with fully fused epiphyses were used.

Acquisition of data

For each complete equid skeleton, the 3D coordinates of anatomical landmarks were registered on 16 bones (scapula, humerus, radio-ulna, metacarpal bone, coxal bone, femur, tibia, calcaneus, talus, metatarsal bone, proximal, middle, and distal phalanges of the fore- and hind limb) using a MICROSCRIBE 3D digitizer. The landmarks were defined according to the protocol of Hanot et al. (2017a) but some landmarks were removed from the analyses (see Supporting Information Data S1).

Shape analyses

A generalized Procrustes Analysis (GPA) was performed on the landmark data of each bone to remove the effects of location, scale, and orientation of the configurations (Rohlf & Slice, 1990). The GPA was performed using the 'R' language and the 'Rmorph' library (Baylac, 2014).

In a previous study performed on the same sample, allometry was demonstrated as statistically significant for all the bones except forelimb phalanges, coxal and metatarsal bones (Hanot et al. 2017b). The results also revealed that the breeds did not share the same allometry, which, coupled with the small size of the sample, would normally make it impossible to remove allometric effects (Klingenberg, 2014). However, allometry is known potentially to contribute greatly to morphological integration (Klingenberg, 2009). Therefore, allometry-free results, obtained by extracting the residuals from a global multivariate regression of the shape against the centroid size of the bones (Monteiro, 1999), were provided for comparison (e.g. Martín-Serra et al. 2015).

Table 1 List of specimens used.

Location	Inventory no.	Sex	Breed	Breed's aptitudes
MNHN-Paris (AC)	MNHN-ZM-AC-1927-235	M	Arabian	Riding-endurance race
IRSNB-Bruxelles	IRSNB-3.975	M	Arabian	Riding-endurance race
ZSM-München	1965-205	F	Arabian	Riding-endurance race
MLU/ZNS/H-Halle	E arb 3	–	Arabian	Riding-endurance race
MNHN-Paris (AC)	MNHN-ZM-AC-1914-337	M	Thoroughbred	Riding-sprint race
ONIRIS-Nantes (AC)	CV9	F	Thoroughbred	Riding-sprint race
ONIRIS-Nantes (AC)	CV1	F	Selle français	Riding-jump races
ONIRIS-Nantes (AC)	CV3	F	Selle français	Riding-jump races
ONIRIS-Nantes (AC)	CV4	F	Selle français	Riding-jump races
ONIRIS-Nantes (AC)	CV2	F	Trotteur français	Riding-trotting race
ONIRIS-Nantes (AC)	CV6	F	Lusitano	Riding-dressage
MNHN-Paris (AC)	MNHN-ZM-AC-1891-107	M	Boulonnais	Draft
MNHN-Paris (AC)	MNHN-ZM-AC-1890-1178	F	Percheron	Draft
MSN-Angers	MHNAn-2010-440	M	Percheron	Draft
NHM-Wien (AZ)	1767	M	Noriker (Pinzgauer)	Draft
NHM-Wien (AZ)	A538	M	Noriker (Pinzgauer)	Draft
MLU/ZNS/H-Halle	E cldd 1	M	Clydesdale	Draft
MLU/ZNS/H-Halle	E cldd 4	F	Clydesdale	Draft
MLU/ZNS/H-Halle	E shr 1	M	Shire	Draft
MNHN-Paris (AC)	MNHN-ZM-AC-1945-27	F	Shetland pony	Riding, light draft
IRSNB-Bruxelles	IRSNB-13.097	F	Shetland pony	Riding, light draft
SAPM-München	SAPM-MA-01141	F	Shetland pony	Riding, light draft
ZSM-München	1963-29	F	Shetland pony	Riding, light draft
MNHN-Paris (AC)	MNHN-ZM-AC-1873-385	F	Icelandic	Riding
MNHN-Paris (AC)	MNHN-ZM-AC-1903-135	–	Icelandic	Riding
MNHN-Paris (AC)	MNHN-ZM-AC-1975-98	M	Icelandic	Riding
ZSM-München	1961-29	F	Icelandic	Riding
IRSNB-Bruxelles	IRSNB-13.071	F	Camargue	Riding
IRSNB-Bruxelles	IRSNB-14.209	-	Pottok	Riding
IRSNB-Bruxelles	IRSNB-16.958	F	Pottok	Riding
IRSNB-Bruxelles	IRSNB-16.959	F	Pottok	Riding
MLU/ZNS/H-Halle	E mgl 1	F	Mongol	Riding, pack, draft
MLU/ZNS/H-Halle	E mgl 2	F	Mongol	Riding, pack, draft
MLU/ZNS/H-Halle	E mgl 3	F	Mongol	Riding, pack, draft
MLU/ZNS/H-Halle	E mgl 4	F	Mongol	Riding, pack, draft

MNHN-Paris (AC), Muséum national d'Histoire naturelle (Comparative Anatomy) – Paris, France; MSN-Angers, Muséum des Sciences naturelles de la ville d'Angers – Angers, France; ONIRIS-Nantes (AC), Ecole Nationale Vétérinaire, Agroalimentaire et de l'Alimentation Nantes-Atlantique (Comparative Anatomy) – Nantes, France; IRSNB-Bruxelles, Institut royal des Sciences naturelles de Belgique – Brussels, Belgium; ZSM-München, Zoologische Staatssammlung München – Munich, Germany; NHM-Wien (AZ), Naturhistorisches museum Wien (Archeological Zoological Collection) – Vienna, Austria; SAPM-München, Staatssammlung für Anthropologie und Paläoanatomie München – Munich, Germany; MLU/ZNS/H-Halle-Halle, Zentralmagazin Naturwissenschaftlicher Sammlungen der Martín-Luther-Unversität Halle-Wittenberg (Museum für Haustierkunde « Julius Kühn ») – Halle (Saale), Germany.

Study of covariation

We studied the covariation between adjacent bones within-limbs (scapula/humerus, humerus/radius-ulna, radius-ulna/metacarpal, metacarpal/proximal forelimb phalanx, proximal/middle forelimb phalanges, middle/distal forelimb phalanges, coxal bone/femur, femur/tibia, tibia/talus, metatarsal bone/talus, metatarsal bone/calcaneus, talus/calcaneus, tibia/metatarsal bone, metatarsal bone/proximal hind limb phalanx, proximal/middle hind limb phalanges, middle/distal hind limb phalanges) and between non-adjacent bones (scapula/radius-ulna, humerus/metacarpal bone, coxal bone/tibia, femur/metatarsal bone) to explore whether functional constraints drive integration patterns.

To assess statistically the significance of covariation, we computed partial least squares (PLS) coefficients (Bookstein et al. 2003). Two block-PLS generates a covariance matrix from the two shape datasets and extracts the principal axes of covariation in order to examine the covariance between them (Rohlf & Corti, 2000). The PLS test refers to a singular warp analysis when applied to geometric shape data (Bookstein et al. 2003). A significant *P*-value was obtained when the observed PLS was higher than those of a distribution of values obtained from randomly permuted blocks and implies that the blocks are significantly integrated. This analysis was computed using the function integration.test included in the 'Geomorph' library (Adams & Otárola-Castillo, 2013). When the covariation between the elements was significant, the first PLS axes were

generated and plotted for each block. All *P*-values were considered statistically significant if below 0.05. 2B-PLS were performed using the 'R' language and the 'Rmorph' library (Baylac, 2014).

To visualize shape deformations associated with these first PLS axes, we used 3D photogrammetric models obtained from the bones of one of the specimens included in the sample (CV9 – ONIRIS-Nantes AC). A set of photographs of each bone were taken from various angles using a Canon EOS 700D. The 3D reconstruction was performed on the software Agisoft PHOTOSCAN (© 2014 Agisoft LLC, 27 Gzhatskaya st., St. Petersburg, Russia) and the 3D surface meshes were imported as 'R' objects using the 'Morpho' library (Schlager, 2016). The landmark coordinates of the 3D models were obtained using the 'Landmark' software (Wiley et al. 2005). A thin plate spline (TPS) deformation of the 3D models was then computed using the 'Morpho' library in order to interpolate the consensus surface. The same function was used to map the extreme shapes of PLS axes via TPS based on the consensus surface as reference. The visualizations displayed in Fig. 9 for three examples of bones were constructed using AVIZO (VSG, Burlington, MA, USA) from the meshes of the extremes shapes of PLS axes. Differences were visualized using color-coded distance maps (blues areas corresponding to the closest surfaces and red ones to the furthest surfaces).

Results

Covariation between forelimb bones

The r_{PLS} shows that there is significant covariation in all the studied pairs of bones except between the metacarpal bone and the proximal forelimb phalanx ($P = 0.14$).

The first axes describe between 75 and 91% of the total shape covariation in the forelimb girdle and long bone pairs (scapula/humerus, scapula/radius-ulna, humerus/radius-ulna, humerus/metacarpal bone and radius-ulna/metacarpal bone). For each bone, the shape covariation associated with the first PLS axes is very similar regardless of the pair in which it is included (Fig. 1A–E). Generally, the morphological change associated with these axes is related to bone robusticity and mainly corresponds to a differential development of the areas for attachment of muscles (e.g. *m. teres major, m. deltoideus, m. triceps brachii* and *m. brachialis*; Fig. 2A–C). This robusticity is also associated, to a lesser extent, to larger articular surfaces and, for some bones (especially the humerus and radius-ulna), to a curved shape of the diaphysis.

The distribution of breeds along the first PLS axis is similar for all these pairs (Fig. 3A–E). In all cases, draft horses clearly separate from the others and present more robust bones. In contrast, the specimens which display the most slender bones are the Icelandic horses, the Pottoks and, to a lesser extent, the Shetland ponies. Race horses generally present an intermediate position with a similar distribution from one pair of bones to another: the Arabian horses present slender bones and pool together with the Nordic horses (Icelandic and Shetland) and Pottoks, whereas the French Saddle horses present more robust bones and the thoroughbreds are intermediate. The Mongol horses are included in the distribution of the race horses and present covariation patterns quite similar to the French Saddle horses corresponding to relatively robust bones. The plots obtained from allometry-free shapes reveal a similar tendency except for the Shetland ponies, and to a lesser extent the Mongolian horses, which display an intermediate position and a greater proximity to the draft horses (Fig. 4A–E).

The first axes describe between 41 and 63% of the total shape covariation in the pairs including forelimb phalanges (proximal/middle and middle/distal phalanges). Once again, for each bone, the shape covariation associated with the first PLS axes is very similar regardless of the pair in which it is included (Fig. 1F,G). Concerning the proximal and middle phalanges, the morphological change associated with these axes is related to the bone robusticity and mainly corresponds to a differential development of the areas for attachment of collateral ligaments and to articular surfaces of variable size (Fig. 2D–F). To a robust middle phalanx is associated a distal phalanx with a proportionally reduced palmar surface, a quite vertical dorsal surface and a dorso-ventrally expanded palmar process.

The distribution of the breeds along the first covariation axis between forelimb phalanges does not follow the same covariation pattern as in the more proximal bones (Fig. 3F, G). Concerning the covariation between the proximal and middle forelimb phalanges, the Shetland ponies are grouped on the negative side of the first PLS axis, which corresponds to robust phalanges. Some of the draft horses tend to pool with the Shetland ponies. The positive side of the PLS axis is bordered by the race horses and the Icelandic ponies, but the Arabian horses tend to depart from the common slope. As previously, the Shetland ponies and some of the draft horses are grouped on the positive side of the first covariation axis between the middle and distal forelimb phalanges. They display a robust middle phalanx and a reduced distal phalanx with a quite vertical dorsal surface and dorso-ventrally expanded palmar process. Race horses are grouped on the positive side corresponding to slender middle phalanx and to a large and flattened distal one. The analyses performed on allometry-free shapes provide a similar distribution of the specimens (Fig. 4F–H).

Covariation between hind limb bones

The r_{PLS} show that there is significant covariation in all the studied pairs except between the coxal bone/femur ($P = 0.28$), the coxal bone/tibia ($P = 0.19$), the talus/calcaneus ($P = 0.06$) and the middle/distal hind limb phalanges ($P = 0.35$).

The first PLS axes describe between 61 and 94% of the total shape covariation in the pairs including hind limb long bones (femur/tibia, femur/metatarsal bone, tibia/metatarsal bone, tibia/talus, metatarsal bone/talus, metatarsal bone/calcaneus). As previously noticed in forelimb bones, the shape covariation associated with the first PLS axis is, for
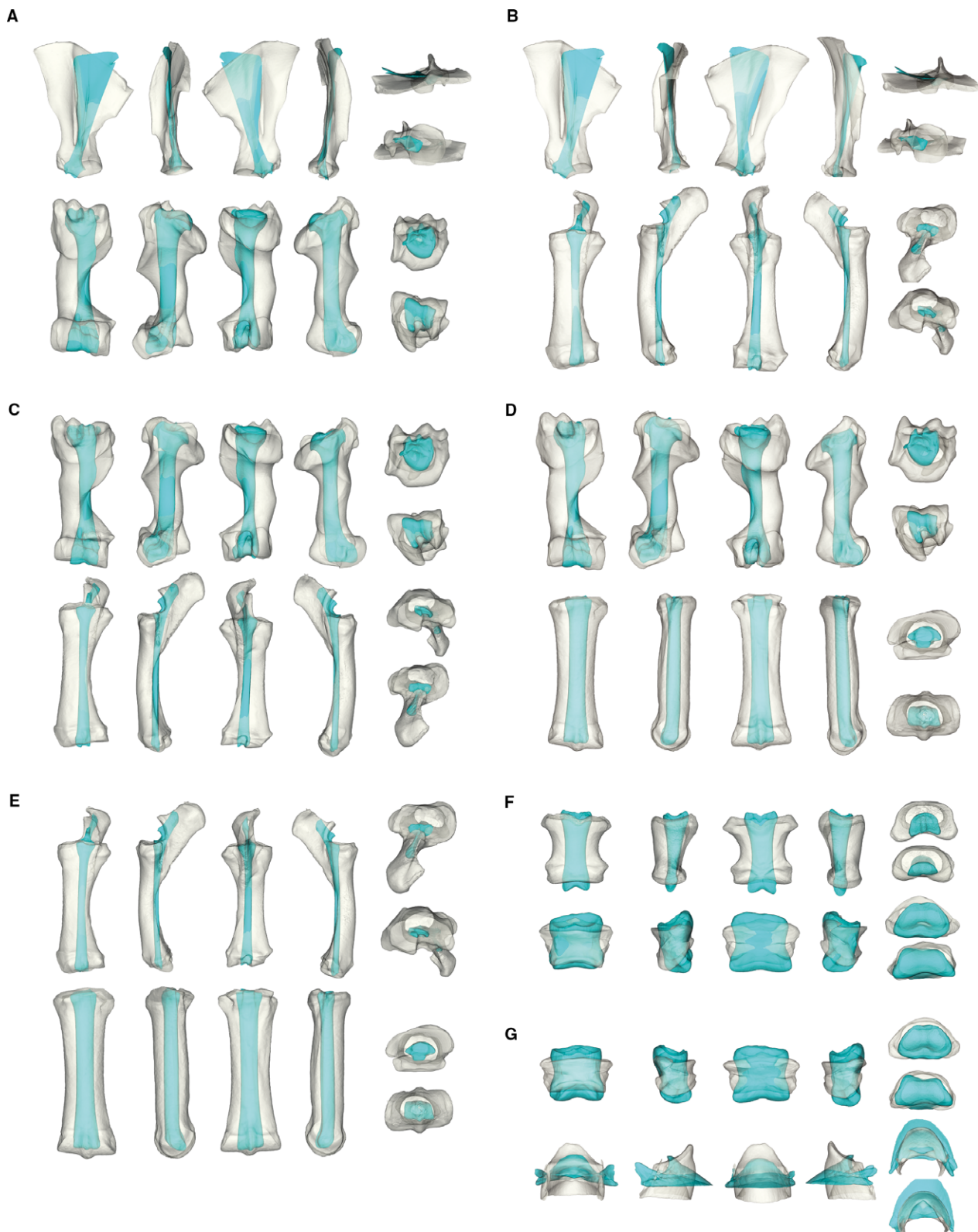
Fig. 1 Shape deformations associated with the first PLS axes between the forelimb bones. (A) scapula and humerus, (B) scapula and radius-ulna, (C) humerus and radius-ulna, (D) humerus and metacarpal bone, (E) radius-ulna and metacarpal bone, (F) proximal and middle forelimb phalanges, (G) middle and distal forelimb phalanges. In white: shape associated with the negative part of the axes; in blue: shape associated with the positive part of the axes.
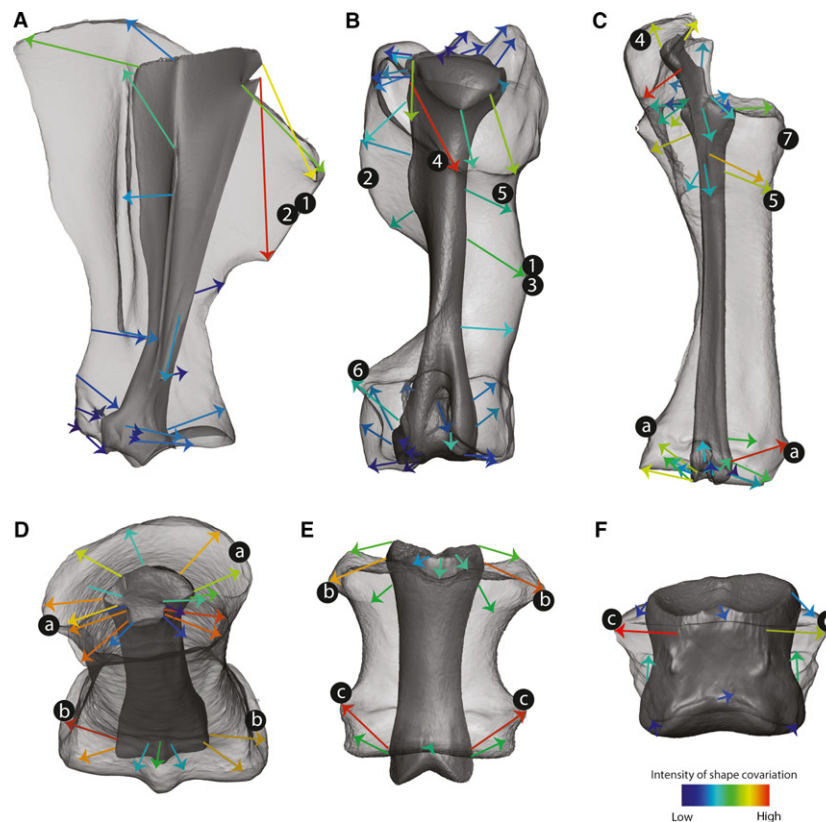
Fig. 2 Shape deformations and vectors associated with the first PLS axes between the forelimb bones. (A) Shape change of the scapula along the scapula-humerus PLS axis, (B) shape change of the humerus along the scapula-humerus PLS axis, (C) shape change of the radius-ulna along the humerus-radius PLS axis, (D) shape change of the metacarpal bone along the radius-metacarpal bone PLS axis, (E) shape change of the proximal forelimb phalanx along the proximal-middle forelimb phalanges PLS axis, (F) shape change of the middle forelimb phalanx along the proximal-middle forelimb phalanges PLS axis. Transparent: shape associated with the negative part of the axes; opaque: shape associated with the positive part of the axes. The color of the arrows corresponds to the intensity of shape deformation along the PLS axis (red: high intensity; blue: low intensity). Numbers and letters respectively correspond to the attachment areas for muscles and for ligaments. 1: *m. teres major*, 2: *m. deltoideus*, 3: *m. latissimus dorsi*, 4: *m. triceps brachii*, 5: *m. brachialis*, 6: *m. extensor carpi radialis*, 7: *m. biceps brachii*; a: collateral ligaments between radius and metacarpal bone, b: collateral ligaments between metacarpal bone and proximal forelimb phalanx, c: collateral ligaments between proximal and middle forelimb phalanges.

each bone, very similar regardless of the pair in which it is included (Fig. 5A–F). Similarly, the morphological change associated with the first covariation axis is mainly related to the bone robusticity with a differential development of the areas for attachment of muscles (*m. gluteus superficialis, m. gastrocnemius, m. biceps femoris* and *m. flexor digitorum longus*; Fig. 6A,B) and with articular sufaces of variable size. A differential curvature is also noticeable on the long bones diaphysis (femur and tibia). The robusticity is associated with the development of the attachment of ligaments concerning the tarsal bones (Fig. 6C–E).

As for the forelimb bones, the draft horses separate from the others due to their robusticity. The Shetland ponies, Icelandic horses and Pottoks present the most slender bones concerning the covariation between the femur and tibia. The covariation in pairs including tarsal bones (tibia/metatarsal bone, tibia/talus, metatarsal bone/talus, metatarsal bone/calcaneus) shows that the Shetland ponies globally present a more intermediate position and display more robust bones than the Icelandic horses. The Arabian horses pool with them, whereas the thoroughbreds and, even more, the French Saddle horses present more robust bones. The major difference with the forelimb bones is the intermediate position of the French Saddle horses between the other race/riding horses and the draft horses. Indeed, the first PLS axis reveals a stronger similarity between the covariation pattern of draft horses and that of the French Saddle Horses which present an association of quite robust bones. As for the forelimb, the allometry-free results reveal a similar tendency to that previously described, except for the Shetland ponies and, to a lesser extent, the Mongolian horses, which are closer to the draft horses (Fig. 8A–D).

The first axes describe between 72 and 90% of the total shape covariation in pairs including hind limb phalanges (metatarsal bone/proximal hind limb phalanx, proximal/middle hind limb phalanges). Once again, for each bone,
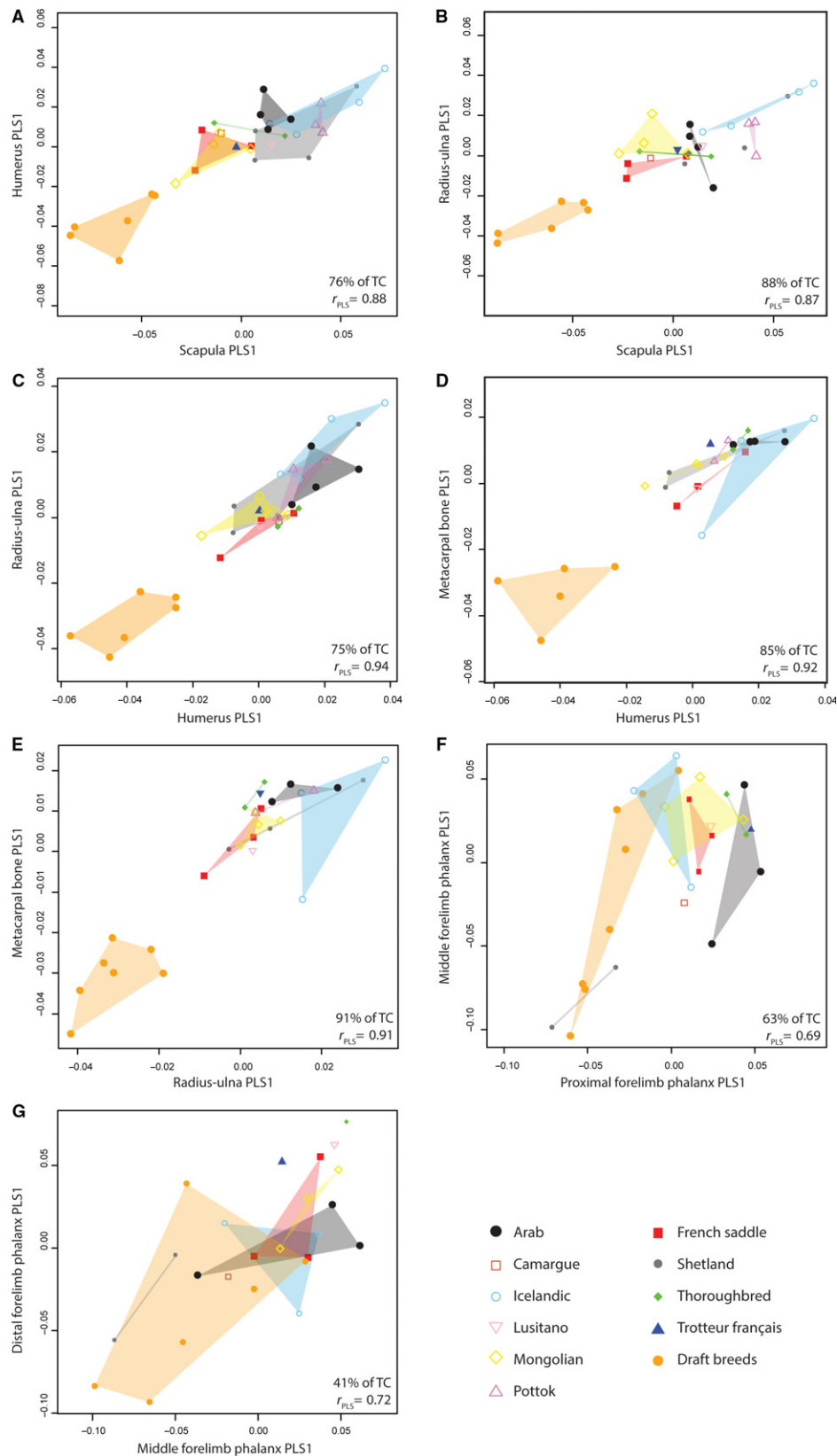
Fig. 3 Scatter plot of the first PLS axes describing covariation between the forelimb bones. (A) Scapula and humerus, (B) scapula and radius-ulna, (C) humerus and radius-ulna, (D) humerus and metacarpal bone, (E) radius-ulna and metacarpal bone, (F) proximal and middle forelimb phalanges, (G) middle and distal forelimb phalanges. r_{PLS}, PLS correlation coefficient; TC, total covariation.
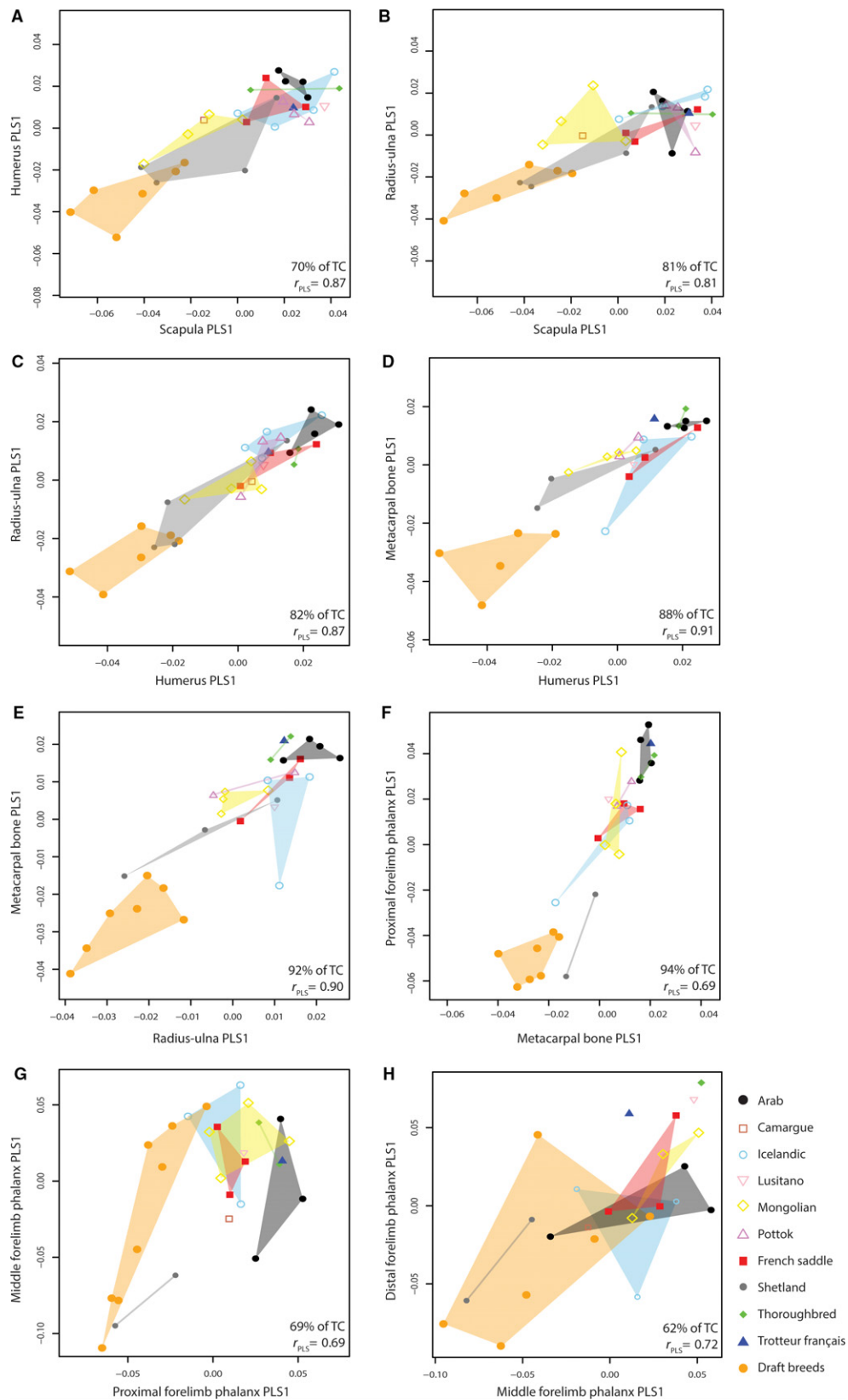
Fig. 4 Scatter plot of the first PLS axes describing covariation between the forelimb bones from allometry-free shapes. (A) Scapula and humerus, (B) scapula and radius-ulna, (C) humerus and radius-ulna, (D) humerus and metacarpal bone, (E) radius-ulna and metacarpal bone, (F) proximal and middle forelimb phalanges, (G) middle and distal forelimb phalanges. r_{PLS}, PLS correlation coefficient; TC, total covariation.
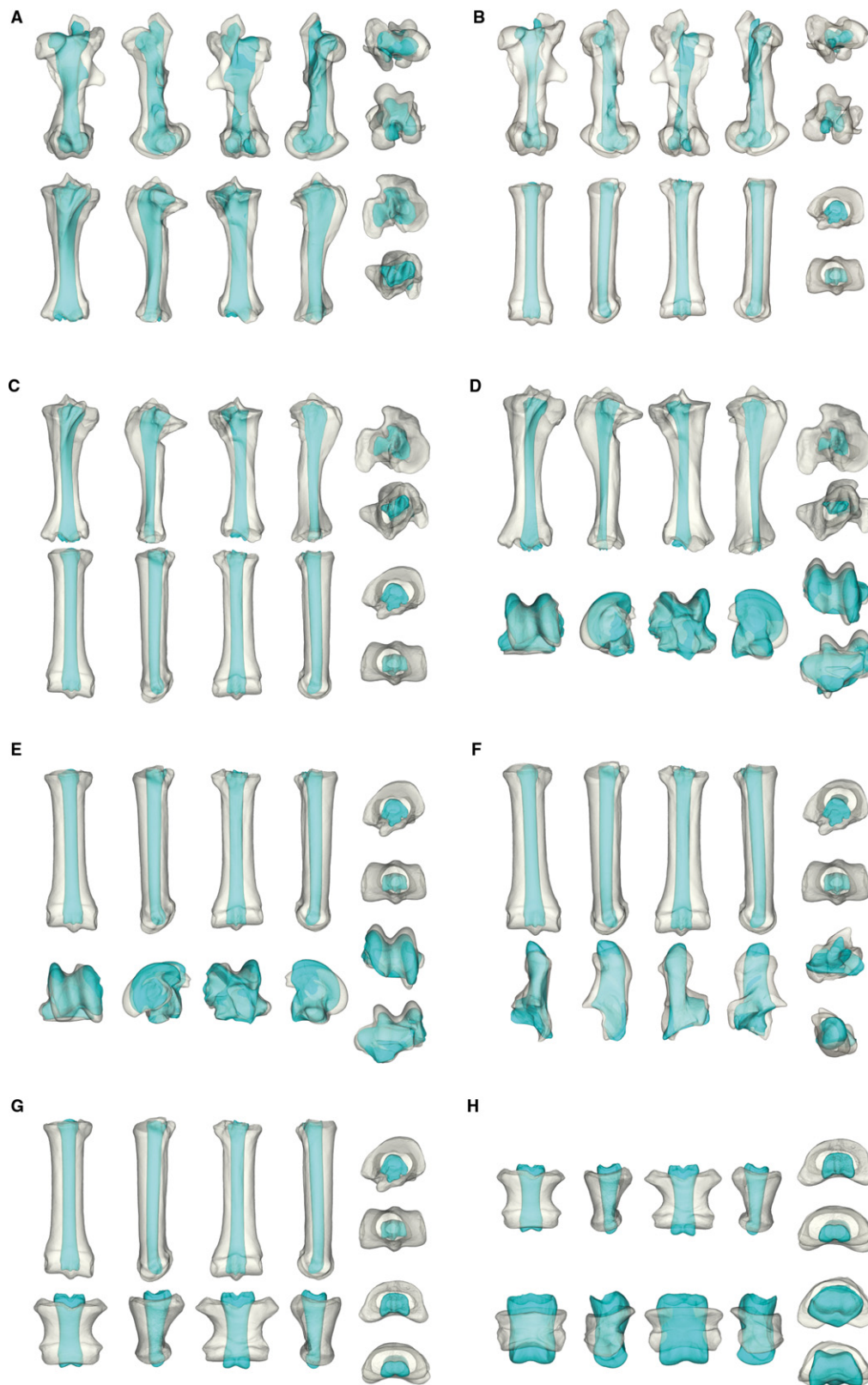
Fig. 5 Shape deformations associated with the first PLS axes between the hind limb bones. (A) Femur and tibia, (B) femur and metatarsal bone, (C) tibia and metatarsal bone, (D) tibia and talus, (E) metatarsal bone and talus, (F) metatarsal bone and calcaneus, (G) metatarsal bone and proximal hind limb phalanx, (H) proximal and middle hind limb phalanges. In white: shape associated with the negative part of the axes; in blue: shape associated with the positive part of the axes.
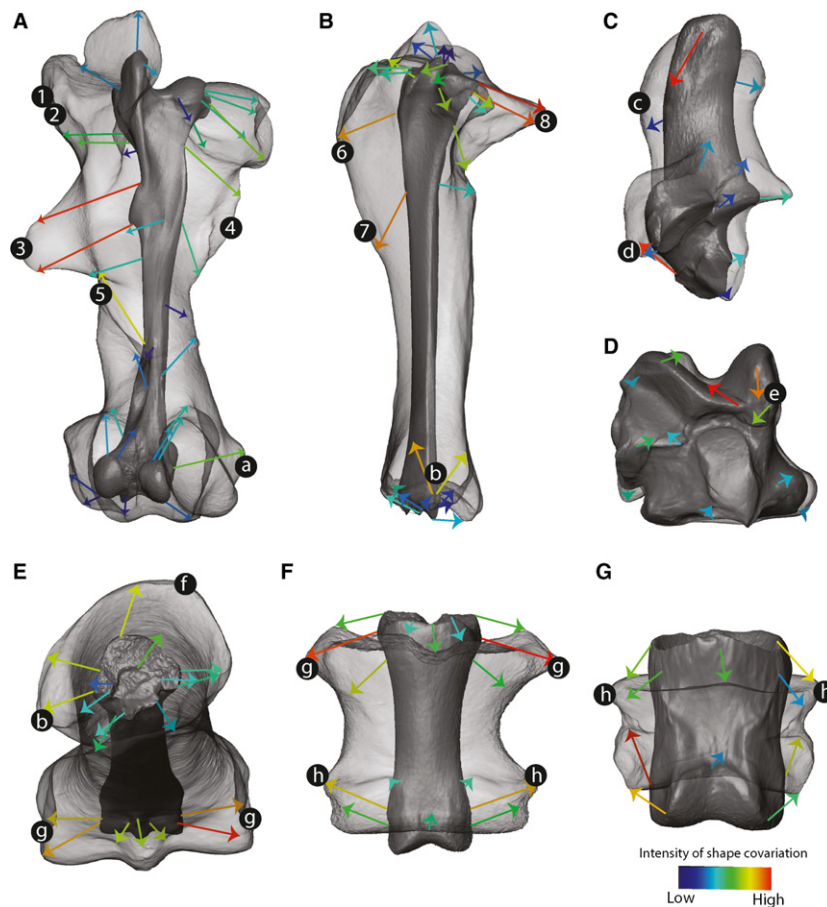
Fig. 6 Shape deformations and vectors associated with the first PLS axes between the hind limb bones. (A) Shape change of the femur along the femur-tibia PLS axis, (B) shape change of the tibia along the femur-tibia PLS axis, (C) shape change of the calcaneus along the metatarsal bone-cal-caneus PLS axis, (D) shape change of the talus along the metatarsal bone-talus PLS axis, (E) shape change of the metatarsal bone along the tibia-metatarsal bone PLS axis, (F) shape change of the proximal hind limb phalanx along the proximal-middle hind limb phalanges PLS axis, (G) shape change of the middle hind limb phalanx along the proximal-middle hind limb phalanges PLS axis. Transparent: shape associated with the negative part of the axes; opaque: shape associated with the positive part of the axes. The color of the arrows corresponds to the intensity of shape deformation along the PLS axis (red: high intensity; blue: low intensity). Numbers and letters respectively correspond to the attachment areas for muscles and for ligaments. 1: *m. gluteus profundus*, 2: *m. gluteus accessorius*, 3: *m. gluteus superficialis*, 4: *m. iliacus* and *m. psoas major*, 5: *m. gastrocnemius*, 6: *m. biceps femoris*, 7: *m. gracilis*, 8: *m. flexor digitorum longus*; a: collateral ligaments between femur and tibia, b: collateral ligaments between tibia and tarsal/metatarsal bones, c: calcaneo-metatarsal ligament, d: tarso-metatarsal ligament, e: plantar talo-calcaneal ligament, f: talo-metatarsal ligament, g: collateral ligaments between metatarsal bone and proximal hind limb phalanx, h: collateral ligaments between proximal and middle forelimb phalanges.

the shape covariation associated with the first PLS axes is very similar regardless of the pair in which it is included (Fig. 5G,H) and corresponds to the bone robusticity with a differential development of the areas for attachment of collateral ligaments (Fig. 6E–G) and articular surfaces of variable size.

The distribution of breeds along the first covariation axis between pairs including hind limb phalanges does not follow the same covariation pattern as in the more proximal bones (Fig. 7G,H). Indeed, similar to the forelimb phalanges, the Shetland ponies and draft horses are grouped on the negative side of the first PLS axis corresponding to associations of robust bones. The Icelandic horses tend to pool with them, whereas other breeds, and particularly race

horses, are pooled at the other end of the axis. As in the forelimb, the results are similar on allometry-free data (Fig. 8E,F).

Discussion

The limbs of the horse: a strongly integrated unit

The fact that the shape change along the first PLS axis is, for each bone, very similar regardless of the pair in which it is included, reveals that each limb operates as a single entity.

Furthermore, the shape deformations along most of the PLS axes show that the principal regions of covariation are
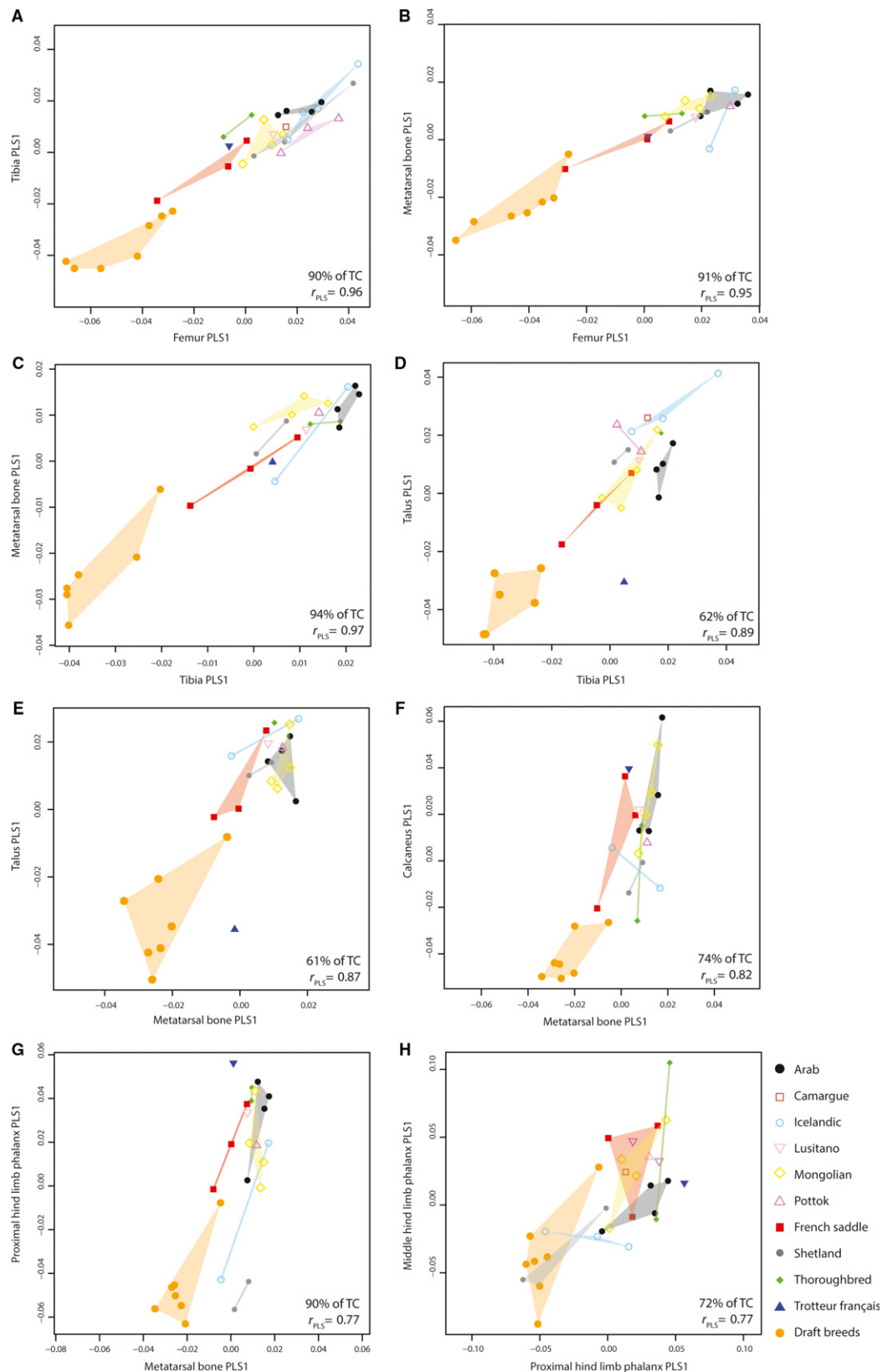
Fig. 7 Scatter plot of the first PLS axes describing covariation between the hind limb bones. (A) Femur and tibia, (B) femur and metatarsal bone, (C) tibia and metatarsal bone, (D) tibia and talus, (E) metatarsal bone and talus, (F) metatarsal bone and calcaneus, (G) metatarsal bone and proximal hind limb phalanx, (H) proximal and middle hind limb phalanges. r_{PLS}, PLS correlation coefficient; TC, total covariation.
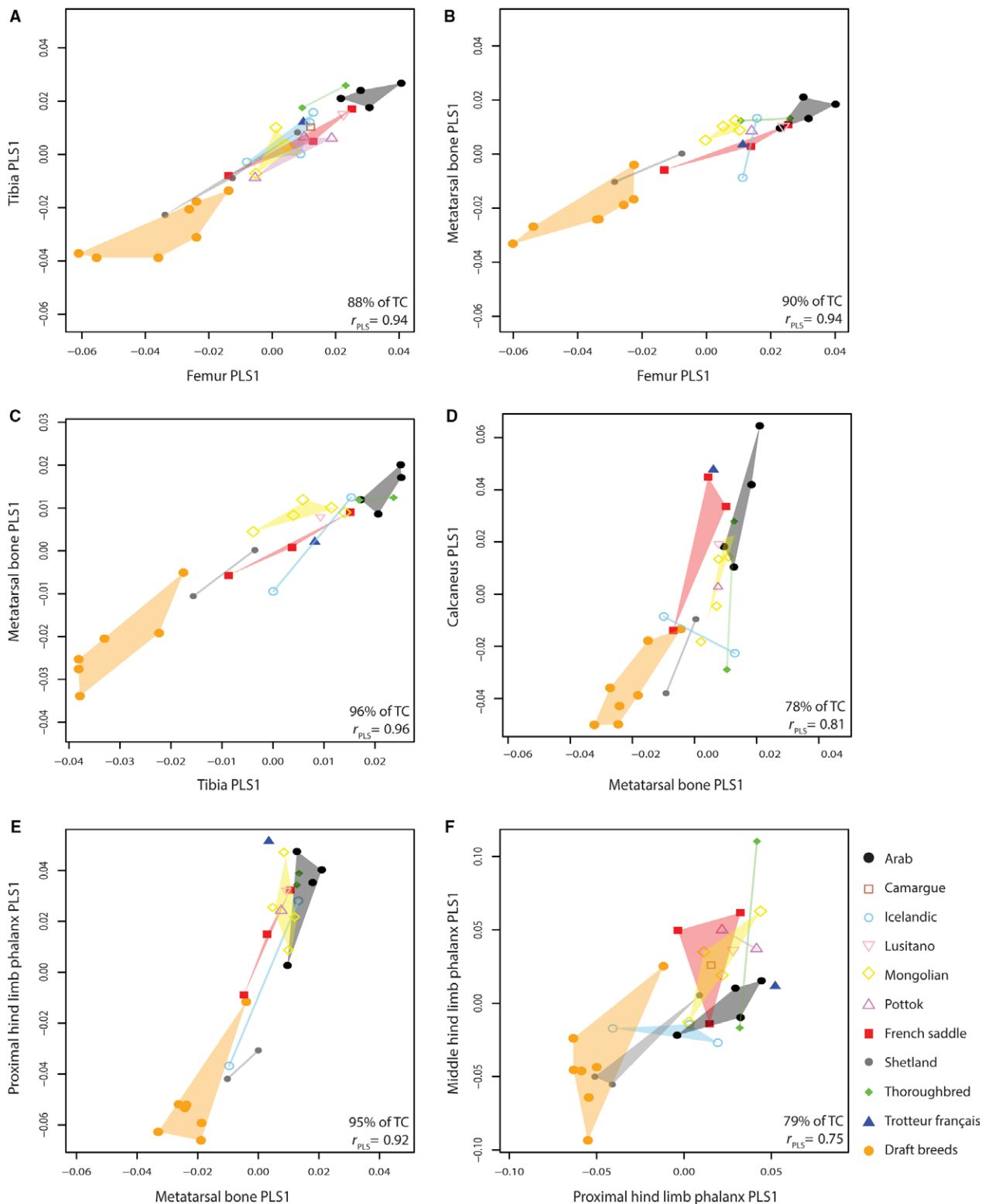
Fig. 8 Scatter plot of the first PLS axes describing covariation between the hind limb bones from allometry-free shapes. (A) Femur and tibia, (B) femur and metatarsal bone, (C) tibia and metatarsal bone, (D) tibia and talus, (E) metatarsal bone and talus, (F) metatarsal bone and calcaneus, (G) metatarsal bone and proximal hind limb phalanx, (H) proximal and middle hind limb phalanges. r_{PLS}, PLS correlation coefficient; TC, total covariation.

located on the diaphyses (essentially the attachment sites of muscles and ligaments) and less on the articular surfaces (Fig. 9). The articular surfaces are involved in the mobility of joints so they tend to covary strongly in taxa which display a wide variety of movements such as rotational movements (e.g. in musteloids; Fabre et al. 2014). Here, the covariation between bones is not due mainly to the anatomical structures implicated in the mobility of the limb (i.e. the articulations) but rather to those providing stability to the articulations (i.e. the muscles and ligaments). This can be related, in horse locomotion, to the required stability of the joints between bones which limit the movements to the parasagittal plane. This low mobility of the articulation joints may partly contribute to the observed strength of morphological integration within the limbs. Each limb could thus be considered a functional unit whose role is centered on parasagittal locomotion. These results are consistent with the previously described strong morphological integration (Hanot et al. 2017b) and demonstrate it from an anatomical point of view.

Shared function as the predominant origin of morphological integration among bones within the same limb

The shape covariation associated with the main PLS axes is, in almost all cases, related to bone robusticity. This result is in accordance with previous studies on mammalian carnivores (Martín-Serra et al. 2015). It should first be noted that bone robusticity goes together, in our results, with large articular surfaces. Since a large area of contact between bones is considered to facilitate load transmission and

dissipation (Ruff, 1988; Fabre et al. 2013), our results could indicate that body mass contributes to produce covariation between bones. Thus, the change in bone robusticity along the PLS axes could be partly related to the impact of body mass and the biomechanical constraints imposed by terrestrial locomotion (Fabre et al. 2013; Martín-Serra et al. 2015). Nevertheless, this change in bone robusticity, observed along the PLS axes, primarily affects the attachment areas for muscles or ligaments. Indeed, the principal regions of covariation between pairs including girdles, stylopods and zeugopods are located on the areas of origin and insertion of muscles. Concerning the autopods (metapodials, tarsal bones and phalanges), the change in bone robusticity is primarily related to the attachment areas of the collateral ligaments (Figs 2–6). This demonstrates that the functional tasks shared by within-limb elements, through common muscles or ligaments, contribute to reinforce morphological covariation. Similarly, along with the development of the attachment areas, the differential curvature of the long bones associated with the covariation axes could also reveal functional interactions. Indeed, it has been suggested that increased bone curvature can accommodate a greater muscle volume or, alternatively, increase bone strains and potentially stimulate remodeling (Lanyon, 1980). According to Milne (2016), increased bone curvature would result from bending strains related to locomotion. Thus, the curvature would be beneficial to counter muscular forces. It has also been suggested that, in terrestrial quadrupeds, the caudal curvature of the radius could be related to the habitual action of the *m. triceps brachii* of maintaining stance (elbow extension) against gravity (Milne, 2016). Similarly, the humerus has been
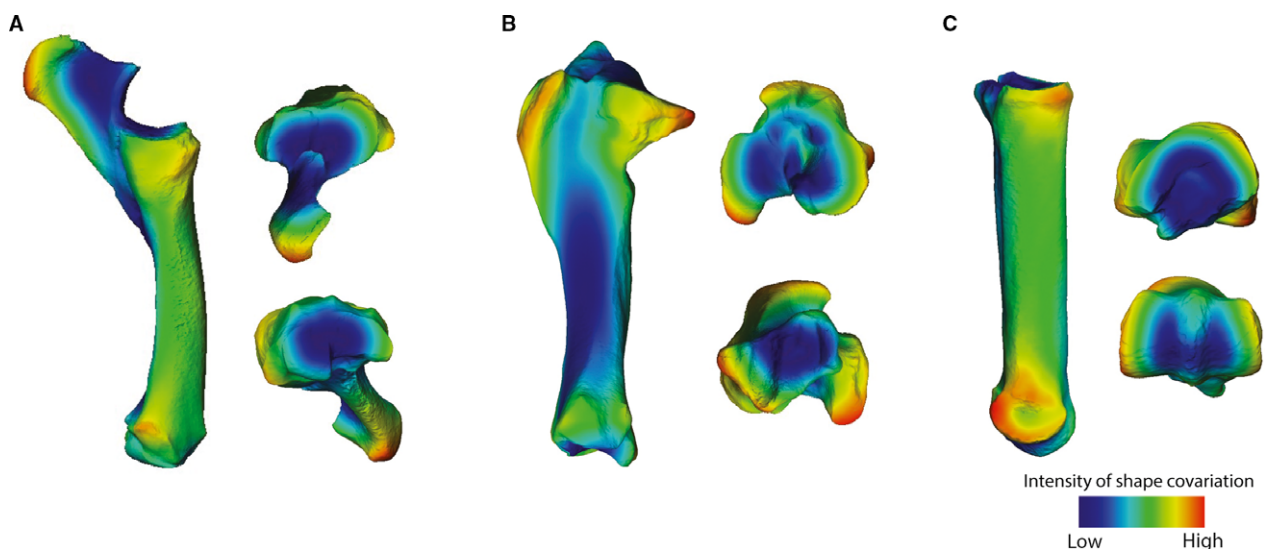

Fig. 9 Anatomical location and intensity of the shape deformation associated with the first PLS axes on three examples of bones. The shape associated with the negative part of the axes was colored according to its distance to the positive part. (A) Shape change of the radius-ulna along the humerus-radius PLS axis, (B) shape change of the tibia along the femur-tibia PLS axis, (C) shape change of the metatarsal bone along the tibia-metatarsal bone PLS axis.

demonstrated to respond to habitual loading (Henderson et al. 2017), which is in agreement with the strong curvature observed in this bone in our sample. In contrast, the metapodials display a straight diaphysis along the entire PLS axes. This allows them to be loaded in axial compression, resulting, at a walking pace, in lower strains than those acting on the radius (Biewener, 1983). Nevertheless, this greater strength implies a lower predictability of the direction of bending strain (Bertram & Biewener, 1988), resulting in a lower resistance with increasing speed and during jumping (Biewener, 1983). In brief, the differential robusticity and curvature of the bones observed along the PLS axes can be considered to reflect a type of morphological integration which is largely related to functional constraints. These results support the hypothesis of Hallgrimsson and colleagues who described covariation among bones within the same limb as primarily the result of functional interactions (Hallgrímsson et al. 2002; Young & Hallgrímsson, 2005).

Furthermore, the results show that, for a given bone, the shape covariation with an adjacent bone is very similar to the shape covariation with a non-adjacent bone with which it shares a muscle (scapula/radius-ulna, humerus/metacarpal bone, femur/metatarsal bone). Sharing muscles implies functional interactions which can be active (via contractile elements) or passive (via passive tendinous structures such as the reciprocal apparatus, which synchronizes motion of the stifle and hock in equids). This further supports the idea that the morphological integration between within-limb elements is largely caused by functional factors.

Impact of selective breeding on covariation patterns

Covariation patterns in pairs including girdle and long bones

Partial least squares analyses indicate that the principal regions of covariation correspond to muscular attachments and one could suppose that the differential development of these attachments areas highlights a differential development of muscles. The distribution of the specimens along the first PLS axes is quite strongly structured according to breeds. This suggests that the diversification in domestic horses, which mainly resulted from artificial selection, impacts covariation patterns, maybe partly with a view to differential muscular development. The sites of muscular attachment are the most developed in draft horses, which present a pattern that is distinct from that observed in other breeds. The results obtained from allometry-free shape data reveal similar tendencies, indicating a relatively low impact of allometry on covariation patterns. This shows that the marked development of muscular insertions in draft horses is not only due to the overall size of the bones and would suggest that the development of muscles may contribute to covariation between girdles/long bones in draft horses. This could be explained by the functional

requirements of tasks attributed to these horses, which have been selected for exerting great and sustained muscular effort. This muscular development can be related with their robust global conformation (Brooks et al. 2010), which is assumed to be under strong selection (Ishizaki et al. 1954; Kashiwamura et al. 2001; Brooks et al. 2010). Our results show that their thickness is not primarily based on body mass but maybe more on the development of muscular mass, given that muscular attachment seems to be affected more by covariation than articular surfaces are.

The results also show a constant distribution within race horses along the first PLS axes: this probably reflects a gradient of increasing muscular development from the Arabian to the French Saddle horses, where the thoroughbreds are found in an intermediate position. The fact that the thoroughbreds display more developed sites for muscle attachment than the Arabian horses is in accord with previous studies which claimed that horses bred for acceleration (such as thoroughbreds in our study) present muscles with greater mass than those bred for endurance (such as Arabian horses; Wagner & Altenberg, 1996). Indeed, greater muscle mass results in a great potential force production and thus the ability to accelerate rapidly (Crook et al. 2008). Our results show that the French Saddle horses present the most developed sites for muscle attachment among race horses. This probably reveals the greater muscular development required in this breed which has been bred for jumping performance. One could suppose that the propulsion forces and mechanisms of impact absorption required in jumping involve robust bones and a greater muscular mass (Langlois et al. 1978). Not surprisingly, the French Saddle horses seem to display an even greater muscular development of the hind limb than of the forelimb, considering their greater proximity to the draft horses on the covariation axes between hind limb bones. This can be explained by the fact that the hind limb is directly responsible for generating propulsion, particularly during jumping (Dutto et al. 2004).

Finally, muscular attachments seem to be the less developed in the Icelandic horses, the Pottoks and some of the Shetland ponies. This would suggest a relatively lower development of muscles than in the other breeds. However, all of these breeds are considered 'ponies' on the basis of their small size (i.e. their height at the withers does not exceed 148 cm; Fédération Equestre Internationale, 2009), which raises the issue of the impact of allometric effects on the apparent low development of muscle insertions. The allometry-free results confirm the respective position of the Pottoks and Icelandic horses but not that of the Shetland ponies, which display an intermediate position, closer to the draft horses. This would suggest that the shape of the muscle insertions in Shetland ponies is related partly to their small size. The position of the Shetland ponies along the PLS axis is nevertheless consistent: indeed, this breed is described as the one displaying the greatest pulling force in

regard to their weight (Cox, 1965). Because of this (coupled with their small size) they are used as light draft horses, especially since the mid-19th century, to work in mines (Hendricks, 2007). However, the Pottoks, which are nowadays used as riding horses, do not display a similar pattern, even though they were also used as pack animal in the past, notably for mining (Hendricks, 2007). In contrast, the Icelandic horses have always been used as saddle animals, which may explain why they pool with the racehorses (Hendricks, 2007).

Finally, the Mongolian horses display an intermediate position along the PLS axis. These horses play a crucial role in nomadic life and are not only used for riding but also extensively as draft or pack animals (Hendricks, 2007). This might explain their greater proximity to the draft horses and the fact that they present more developed attachment areas for muscles, suggesting a potentially greater muscular mass. The results obtained for the allometry-free shapes emphasize this tendency even more.

Covariation patterns in autopods

The distribution of the specimens along the first covariation axes between pairs including phalanges is poorly structured according to breeds. Moreover, some specimens tend to diverge from the common slope, revealing more diversified covariation patterns between distal bones than proximal ones. This result is in agreement with the idea that autopods would be more variable than the proximal bones of the limbs due to their direct contact with the ground, causing a greater sensitivity to environmental pressures (Hallgrímsson et al. 2002). In addition, the proximo-distal direction of limb development may cause accumulation of variation in the distal parts (Dudley et al. 2002; Sun et al. 2002; Tickle & Wolpert, 2002; Wolpert, 2004).

The principal regions of covariation for proximal and middle phalanges correspond to the attachment of the collateral ligaments (Figs 2–6). Concerning the first PLS axis between middle and distal phalanges, the results reveal that a robust middle phalanx is associated with a distal phalanx with a proportionally reduced palmar surface, a rather vertical dorsal surface and a dorso-ventrally expanded palmar process. This tends to confirm that the conformation of the distal phalanx impacts the strains on the ligaments (Leach, 1993), probably producing their differential development.

In spite of the breeds being less distinct along the first PLS axes, some tendencies were detected. Indeed, the ligament insertion areas of the proximal and middle phalanges are the most developed in some draft horses and Shetland ponies, which also display short distal phalanges with dorso-ventrally expanded palmar process.

The lesser development of the attachment areas in riding horses could be related to an adaptation to fast gait speeds: indeed, the ligaments play a role in elastic energy recovery (especially during running), and energy saving is considered as favored by long and thin ligaments (Biewener, 1998).

Moreover, a previous study described a peculiar hoof conformation in draft horses with a greater toe height and a large hoof angle (Gabriel et al. 1997). This conformation was hypothesized by the authors to contribute to reducing the strain of the *m. flexor digitorum longus* tendon on the distal bones. Thus, this foot configuration was presented as well adapted to a great body mass. In spite of the fact that the correlation between the hoof capsule and bone shapes is generally depicted as modest (Cruz et al. 2006; Dyson et al. 2011), our results for distal phalanges agree with the description of the hoof conformation in draft horses by Gabriel et al. (1997). Moreover, this peculiar distal phalanx conformation is associated with robust middle phalanges, in agreement with the hypothesis of an important role of body mass in shaping the distal phalanx. Indeed, a great body mass probably requires strong joint stability with a strong ligament development. Gabriel et al. (1997) also observed a similar hoof conformation between the draft horses and the light ponies concerning the high ratio between heel height and toe height. Our results corroborate this finding considering the similar phalangeal covariation patterns in the draft horses and the Shetland ponies. The probable need for increased joint stability is also apparent in the tarsal joint of the Shetland ponies, with bones displaying relatively strongly developed areas for ligament attachment. This similarity with draft horses may be related to the robust global conformation of the Shetland pony (Brooks et al. 2010), which would imply an adaptation of the distal parts to their relative great body mass. It may also be related to the sure-footed locomotion required to move around the hard and rocky grounds of their islands of origin (Lynghaug, 2009)., Similarly, whereas the large hooves of the French Saddle Horses are considered particularly suitable for landing jumps, it is likely that a small foot would be well adapted to difficult terrain (Pagnier, 1821).

Conclusion

This study explores the patterns of integration in the limb bones of different horse breeds. The results are in agreement with existing hypotheses suggesting that within-limb integration would mainly result from functional interactions: indeed, the principal regions of shape covariation are related to the action of muscles and ligaments through differential development of the attachment areas or bending of the diaphysis. Horse locomotion being limited to a parasagittal plane, each limb seems to function as a whole unit, resulting in strong overall integration. Our results also highlight that covariation patterns are strongly structured by breed. This suggests that diversification in domestic horses, which mainly stems from selective breeding, impacts covariation patterns. Concerning the long bones and girdles, selection seems to modulate covariation patterns that correspond to differential muscular development. Draft horses clearly diverge from the other breeds with a

covariation primarily driven by the action of strongly developed muscles. The covariation between autopodial bones is mostly related to the ligament development, suggesting an impact on joint stability or on running abilities. Contrary to pairs of proximal bones, Shetland ponies group with draft horses and present robust autopods which probably reflect some function-specific traits. These data attest to the impact of artificial selection on covariation patterns, even within strongly integrated structures. They demonstrate the ability of micro-evolutionary processes to modulate covariation patterns. Future studies would benefit from exploring these issues across a wider range of domestic taxa. Moreover, the issue of the impact of bone plasticity on integration patterns should also be addressed using specimens for which usages and activities during the lifespan are documented.

Acknowledgements

Conflict of interest

The authors declare no conflict of interest.

Author contributions

P.H. carried out the acquisition of data, performed the statistical analyses and drafted the manuscript. A.H. contributed to conception of the study, interpretation of data and drafting the manuscript. C.G. contributed to collecting data and to interpretation of data. R.C. contributed to conception, statistical analysis and interpretation of data. All authors revised and approved the manuscript.

References

Adams DC (2016) Evaluating modularity in morphometric data: challenges with the RV coefficient and a new test measure. *Methods Ecol Evol* **7**, 565–572.

Adams DC, Otárola-Castillo E (2013) geomorph: an R package for the collection and analysis of geometric morphometric shape data. *Methods Ecol Evol* **4**, 393–399. https://doi.org/10.1111/2041-210X.12035.

Baylac M (2014) Rmorph: A R Geometric and Multivariate Morphometrics Library. Michel Baylac, Paris

Bertram JEA, Biewener AA (1988) Bone curvature: sacrificing strength for load predictability? *J Theor Biol* **131**, 75–92. https://doi.org/10.1016/S0022-5193(88)80122-X.

Biewener AA (1983) Allometry of quadrupedal locomotion: the scaling of duty factor, bone curvature and limb orientation to body size. *J Exp Biol* **105**, 147–171.

Biewener AA (1998) Muscle-tendon stresses and elastic energy storage during locomotion in the horse. *Comp Biochem Physiol B Biochem Mol Biol* **120**, 73–87.

Bookstein FL, Gunz P, Mitterœcker P, et al. (2003) Cranial integration in *Homo*: singular warps analysis of the midsagittal plane in ontogeny and evolution. *J Hum Evol* **44**, 167–187.

Brooks SA, Makvandi-Nejad S, Chu E, et al. (2010) Morphological variation in the horse: defining complex traits of body size and shape. *Anim Genet* **41**, 159–165.

Cheverud JM (1982) Phenotypic, genetic, and environmental morphological integration in the cranium. *Evolution* **36**, 499–516.

Cox MC (1965). The Shetland Pony. Black.

Crook TC, Cruickshank SE, McGowan CM, et al. (2008) Comparative anatomy and muscle architecture of selected hind limb muscles in the Quarter Horse and Arab. *J Anat* **212**, 144–152.

Cruz CD, Thomason JJ, Faramarzi B, et al. (2006) Changes in shape of the Standardbred distal phalanx and hoof capsule in response to exercise. *Equine Comp Exerc Physiol* **3**, 199–208.

Darwin C (1868) *The Variation of Animals and Plants under Domestication*. London: J. Murray.

Denis B (2012) Les races de chevaux en France au XVIIIe siècle. Et les idées relatives à leur amélioration. *Situ Rev Patrim* **18**, [online].

Drake AG, Klingenberg CP (2010) Large-scale diversification of skull shape in domestic dogs: disparity and modularity. *Am Nat* **175**, 289–301.

Dudley AT, Ros MA, Tabin CJ (2002) A re-examination of proximodistal patterning during vertebrate limb development. *Nature* **418**, 539–544.

Dutto DJ, Hoyt DF, Clayton HM, et al. (2004) Moments and power generated by the horse (*Equus caballus*) hind limb during jumping. *J Exp Biol* **207**, 667–674.

Dyson SJ, Tranquille CA, Collins SN, et al. (2011) An investigation of the relationships between angles and shapes of the hoof capsule and the distal phalanx. *Equine Vet J* **43**, 295–301.

Fabre A-C, Cornette R, Peigné S, et al. (2013) Influence of body mass on the shape of forelimb in musteloid carnivorans. *Biol J Linn Soc* **110**, 91–103.

Fabre A-C, Goswami A, Peigné S, et al. (2014) Morphological integration in the forelimb of musteloid carnivorans. *J Anat* **225**, 19–30.

Fédération Equestre Internationale (2009) *Rules for dressage events*, 23rd edn. Lausanne:Fédération Equestre Internationale.

Gabriel A, Detilleux J, Jolly S, et al. (1997) Etude morphométrique du sabot et du petit sésamoïde du cheval. *Ann Méd Vét* **147**, 319–340.

Goswami A, Polly PD (2010) The influence of modularity on cranial morphological disparity in carnivora and primates (Mammalia). *PLoS ONE* **5**, e9517.

Goswami A, Smaers JB, Soligo C, et al. (2014) The macroevolutionary consequences of phenotypic integration: from development to deep time. *Philos Trans R Soc B* **369**, 20130254.

Hallgrímsson B, Willmore K, Hall BK (2002) Canalization, developmental stability, and morphological integration in primate limbs. *Am J Phys Anthropol* **119**, 131–158.

Hallgrímsson B, Jamniczky H, Young NM, et al. (2009) Deciphering the Palimpsest: Studying the Relationship Between Morphological Integration and Phenotypic Covariation. *Evol Biol* **36**, 355–376.

Hanot P, Herrel A, Guintard C, et al. (2017a) Morphological integration in the appendicular skeleton of two domestic taxa: the horse and donkey. *Proc R Soc B* **284**, 20171241.

Hanot P, Guintard C, Lepetz S, et al. (2017b) Identifying domestic horses, donkeys and hybrids from archaeological deposits: a 3D morphological investigation on skeletons. *J Archaeol Sci* **78**, 88–98.

Henderson K, Pantinople J, McCabe K, et al. (2017) Forelimb bone curvature in terrestrial and arboreal mammals. *PeerJ* **5**, e3229.

Hendricks BL (2007) *International Encyclopedia of Horse Breeds.* Norman, OK: University of Oklahoma Press.

Ishizaki S, Honzawa S, Shinohara A, et al. (1954) Relation between body weight and work power in the horse. *Nihon Chikusan Gakkaiho* **25**, 168–173.

Kashiwamura F, Avgaandorj A, Furumura K (2001) Relationships among body size, conformation, and racing performance in Banei draft racehorses. *J Equine Sci* **12**, 1–7.

Klingenberg CP (2009) Morphometric integration and modularity in configurations of landmarks: tools for evaluating a priori hypotheses. *Evol Dev* **11**, 405–421.

Klingenberg CP (2013) Cranial integration and modularity: insights into evolution and development from morphometric data. *Hystrix Ital J Mammal* **24**, 43–58.

Klingenberg CP (2014) Size, shape, and form: concepts of allometry in geometric morphometrics. *Dev Genes Evol* **226**, 113–137.

Langlois B, Froidevaux J, Lamarche L, et al. (1978) Analyse des liaisons entre la morphologie et l'aptitude au galop au trot et au saut d'obstacles chez le Cheval. *Ann Génét Sélect Anim* **10**, 443–474.

Lanyon LE (1980) The influence of function on the development of bone curvature. An experimental study on the rat tibia. *J Zool* **192**, 457–466.

Lawler RR (2008) Morphological integration and natural selection in the postcranium of wild verreaux's sifaka (*Propithecus verreauxi verreauxi*). *Am J Phys Anthropol* **136**, 204–213.

Leach DH (1993) Treatment and pathogenesis of navicular disease ('syndrome') in horses. *Equine Vet J* **25**, 477–481.

Lizet B (1989) *La Bête noire: À la recherche du cheval parfait.* Paris: Les Editions de la MSH.

Lynghaug F (2009) *The Official Horse Breeds Standards Guide: The Complete Guide to the Standards of All North American Equine Breed Associations.* Saint Paul: MBI Publishing Company.

Magwene PM (2001) New tools for studying integration and modularity. *Evolution* **55**, 1734–1745.

Marroig G, Cheverud JM (2001) A comparison of phenotypic variation and covariation patterns and the role of phylogeny, ecology, and ontogeny during cranial evolution of new world monkeys. *Evolution* **55**, 2576–2600.

Martín-Serra A, Figueirido B, Pérez-Claros JA, et al. (2015) Patterns of morphological integration in the appendicular skeleton of mammalian carnivores. *Evolution* **69**, 321–340.

Milne N (2016) Curved bones: an adaptation to habitual loading. *J Theor Biol* **407**, 18–24.

Mitteroecker P, Bookstein F (2007) The Conceptual and Statistical Relationship between Modularity and Morphological Integration. *Syst Biol* **56**, 818–836.

Monteiro LR (1999) Multivariate regression models and geometric morphometrics: the search for causal factors in the analysis of shape. *Syst Biol* **48**, 192–199.

Mulliez J (1983). Les Chevaux du Royaume. Histoire de l'élevage du cheval et de la création des haras.Paris:Montalba.

Musset R (1917) L'élevage du cheval en France.Paris:Librairie Agricole de la Maison Rustique

Olson EC, Miller RL (1958) *Morphological Integration.* Chicago, IL: University of Chicago Press.

Olson EC, Miller RL (1951) A Mathematical Model Applied to a Study of the Evolution of Species. *Evolution* **5**, 325–338.

Pagnier C-J (1821) *Théorie de l'extérieur du cheval: Précédée d'un abrégé des os qui forment le squelette, et d'une nomenclature des principaux organes.* Paris: Madame Huzard.

Rohlf FJ, Corti M (2000) Use of two-block partial least-squares to study covariation in shape. *Syst Biol* **49**, 740–753.

Rohlf FJ, Slice D (1990) Extensions of the procrustes method for the optimal superimposition of landmarks. *Syst Biol* **39**, 40–59.

Rolian C (2009) Integration and evolvability in primate hands and feet. *Evol Biol* **36**, 100–117.

Ruff C (1988) Hindlimb articular surface allometry in hominoidea and *Macaca*, with comparisons to diaphyseal scaling. *J Hum Evol* **17**, 687–714.

Schlager S (2017) Morpho and Rvcg–shape analysis in R. In: *Statistical Shape and Deformation Analysis* (eds Zheng G, Li S, Szekely G), pp. 217–256. Cambridge: Academic Press.

Sponenberg DP (2000) Genetic resources and their conservation. In: *The Genetics of the Horse* (eds Bowling AT, Ruvinsky A), pp. 387–438. Wallingford: CABI.

Sponenberg DP, Christman C (1995) A Conservation Breeding Handbook. Pittsboro:American Livestock Breeds Conservancy.

Sun X, Mariani FV, Martin GR (2002) Functions of FGF signalling from the apical ectodermal ridge in limb development. *Nature* **418**, 501–508.

Tickle C, Wolpert L (2002) The progress zone – alive or dead? *Nat Cell Biol* **4**, E216–E217.

Van Valen L (1965) The study of morphological integration. *Evolution* **19**, 347–349.

Wagner GP, Altenberg L (1996) Perspective: complex adaptations and the evolution of evolvability. *Evolution* **50**, 967–976.

Wagner GP, Pavlicev M, Cheverud JM (2007) The road to modularity. *Nat Rev Genet* **8**, 921–931.

Wiley DF, Amenta N, Alcantara DA, et al. (2005) Evolutionary morphing. In: *VIS 05. IEEE Visualization, 2005. Presented at the VIS 05. IEEE Visualization, 2005*, pp. 431–438.

Wolpert L (2004) The progress zone model for specifying positional information. *Int J Dev Biol* **46**, 869–870.

Young NM, Hallgrímsson B (2005) Serial homology and the evolution of mammalian limb covariation structure. *Evolution* **59**, 2691–2704.

Young NM, Wagner GP, Hallgrímsson B (2010) Development and the evolvability of human limbs. *Proc Natl Acad Sci U S A* **107**, 3400–3405.

Supporting Information

Additional Supporting Information may be found in the online version of this article:

Data S1. Definition of the landmarks used in the analysis.